PASJ: Publ. Astron. Soc. Japan **46**, 375–394 (1994)

Spectral Evolution of the Bright X-Ray Nova GS 1124−68 (Nova Muscae 1991) Observed with Ginga

Ken EBISAWA,[1,2] Mina OGAWA,[3] Takashi AOKI, Tadayasu DOTANI, Mamoru TAKIZAWA, Yasuo TANAKA, and Kenji YOSHIDA[4]
Institute of Space and Astronautical Science, 3-1-1, Yoshinodai, Sagamihara, Kanagawa 229
E-mail (KE) ebisawa@bluejay.gsfc.nasa.gov
and
Shigenori MIYAMOTO, Sayuri IGA,[5] Kiyoshi HAYASHIDA, Shunji KITAMOTO, and Kentaro TERADA
Department of Earth and Space Science, Department of Physics, Faculty of Science, Osaka University, 1-1 Machikaneyama-cho, Toyonaka, Osaka 560

(Received 1993 November 12; accepted 1994 March 10)

Abstract

A bright X-ray nova, GS 1124−68 (Nova Muscae 1991, GRS 1124−68), which later turned out to be a promising black-hole binary with evidence of large mass, was observed with the Large Area Counters onboard Ginga from its discovery in 1991 January to its quiescent state in 1991 September. The X-ray intensity reached a maximum ($\sim$ 8 Crab) eight days after its discovery, then decreased exponentially with an e-folding time of about $\sim$ 30 d. Temporary increases in the luminosity were found $\sim$ 80 d and $\sim$ 200 d after the outburst. The source was last detected at $\sim$ 2 mCrab on the 239th day after the outburst; although subsequent observations were carried out on days 260 and 282, the source was below the detection limit ($\sim$ 0.3 mCrab). GS 1124−68 exhibited such a drastic state transition that was very reminiscent of the high-low transition of black-hole candidates Cyg X-1 and GX 339−4, between the 131st day (May 18) and 157th day (June 13) after the outburst. Before the transition, the energy spectrum was characterized by a thermal soft component which was dominant below $\sim$ 8 keV, and a power-law like hard-tail component, which was significant above that energy. After the transition, the energy spectrum became much harder. The spectrum was approximately represented by a single power-law function with a photon index of $\sim$ 1.7. Intense short time variations, which were quite similar to those in the low state of Cyg X-1, GX 339−4 and GS 2023+338, became prominent down to a timescale of milliseconds. The outburst mechanism, the origin of the soft component and the state transition can be favorably explained in terms of an optically thick accretion-disk model around a $\sim 6M_\odot$ black-hole at a distance of $\sim$ 2.5 kpc.

Key words: Accretion disks — Binaries — Black holes — Novae — X-rays: stars

1. Introduction

On 1991 January 8, a bright X-ray nova was discovered in the Musca constellation with all sky monitors on board both the Ginga and GRANAT satellites (Makino, Ginga team 1991; Lund, Brandt 1991; Kitamoto et al. 1992; Brandt et al. 1992). The nova was named GS 1124−68/GRS 1124−68. Optical identification was subsequently carried out, and the characteristics of the optical star suggested that the source is a low-mass binary system (Della Valle et al. 1991a, 1991b). Optical photometry and spectroscopy revealed a 10.4-day orbital period and a mass-function value of $3.1M_\odot$ (Remillard et al. 1992). Because of the large mass function, which is a conservative lower limit of the mass of the compact object, GS 1124−68 is considered to be a binary system comprising a black-hole and a low-mass companion, just like X-ray novae A0620−00 (McClintock, Remillard 1986) and GS 2023+338 (Casares et al. 1992).

Black-hole candidates have several X-ray characteristics which are not found in neutron-star binaries (for a review, e.g., Tanaka 1989; Inoue 1992). There are two distinct spectral states: the soft spectral state and the hard spectral state. In the soft spectral state, the X-ray energy spectra are characterized by a much lower temperature ("ultra-soft" energy spectra) than those for

1 Present Address: code 668, Laboratory for High Energy Astrophysics, NASA/Goddard Space Flight Center, Greenbelt, MD 20771, U.S.A.
2 Also Universities Space Research Association.
3 Present Address: NASDA, Hatoyama, Saitama 350-03.
4 Present Address: Faculty of Engineering, Kanagawa University, 3-27-1 Rokkakubashi, Kanagawa-ku, Yokohama, Kanagawa 221.
5 Present Address: Hitachi ltd. Totsuka-ku, Yokohama, Kanagawa 224.

neutron-star sources (White et al. 1984; White, Marshall 1984). On the other hand, in the hard spectral state, the energy spectra are much harder than those of neutron-star sources, and are roughly expressed with a power-law function with a photon index of $\sim$ 1.7 over 2–30 keV. Short timescale variations down to milliseconds are quite remarkable in the hard spectral state, while they are much weaker in the soft spectral state. Some black-hole candidates, such as Cyg X-1 and GX 339−4, exhibit a state transition such that they are in the soft spectral state when the X-ray luminosity is relatively high, and in the hard spectral state when the luminosity is low. Being an X-ray nova, GS 1124−68 has undergone large changes in its mass accretion rate, and, hence, provides the best opportunity to study the spectral variations of a certain black-hole candidates accompanying large luminosity changes.

Between 1991 January and October, GS 1124−68 was intermittently observed with the Large Area Counters on-board Ginga (Turner et al. 1989) in addition to regular monitoring with the All Sky Monitor (Kitamoto et al. 1992). In this paper, we report on the results of the LAC observations of GS 1124−68, with main emphasis placed on its spectral evolution. The results of a timing study are separately presented (Dotani 1992; Miyamoto et al. 1993).

Hard X-ray observations were also carried out with the ART-P (3–30 keV) and SIGMA (35–1300 keV) telescopes on board GRANAT over the entire outburst period. These GRANAT results can be found in Gil'fanov et al. (1991), Sunyaev et al. (1992), Goldwurm et al. (1992), Gil'fanov et al. (1993), Goldwurm et al. (1993), and Lund (1993).

2. Observations

GS 1124−68 was discovered by the Ginga ASM during a routine scan at 18:50–19:00 on 1991 January 8. The source was below the ASM detection limit ($\sim$ 50 mCrab) in the previous scan on January 5. In order to determine the position accurately, LAC scan observations were carried out on January 10. Subsequently, LAC pointing observations were occasionally made until 1991 October 17, with intervals of a few days to one month. For each observation, data were taken with different observational modes to study both the energy spectra and any fast time variations. In this work, we used the MPC1 or MPC2 data (48 PHA channels) to study the energy spectra, and the MPC3 data (12 PHA channels and 8 ms time resolution) to study the fast time variability. Only the data within an energy range of 1.2–37 keV were selected for analysis.

In figure 1, a light curve of GS 1124−68 taken with LAC is shown together with those of bright black-hole candidates novae A0620−00, GS 2000+25, and GS 2023+338. GS 1124−68 was last detected on September 3 (239 d after the outburst) at $\sim$ 2 mCrab. Although subsequent pointing and scanning observations were carried out on September 24th (260 d) and October 16th (282 d), the source was below the detection limit ($\sim$ 0.3 mCrab).

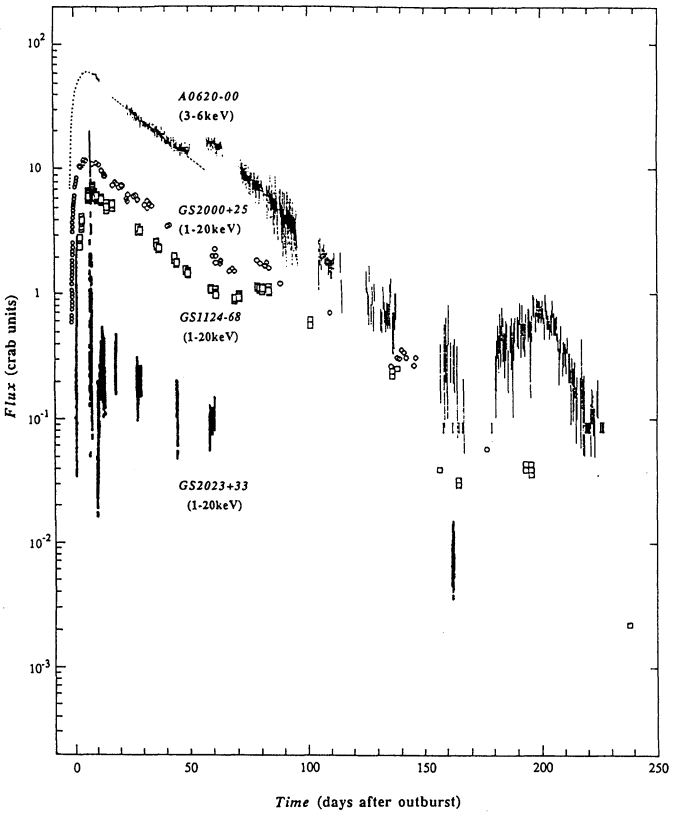

Fig. 1. Light curve of GS 1124−68 taken with LAC together with those of black-hole candidates novae A0620−00 (Elvis et al. 1975; Kalzienski et al. 1977), GS 2000+25 (Tsunemi et al. 1989), and GS 2023+33 (Kitamoto et al. 1990). Note the similarities of these light curves: (1) $\sim$ 3 d rise time (GS 1124−68, A0620−00, and GS 2000+25); (2) logarithmic decay with a decay time of $\sim$ 30 days (all the sources); and (3) the second hump on 60–90 d after the outburst (GS 1124−68, A0620−00, and GS 2000+25) and the additional third hump on $\sim$ 200 d after the outburst (GS 1124−68 and A0620−00).

3. Analysis and Results

3.1. Light Curve

The long-term intensity variation of GS 1124−68 (figure 1) exhibits the following distinguished characteristics shared with the other black-hole candidates novae shown together (see Kitamoto et al. 1992 for the ASM results): (1) After the discovery on January 8 at $\sim$ 0.8 Crab, the

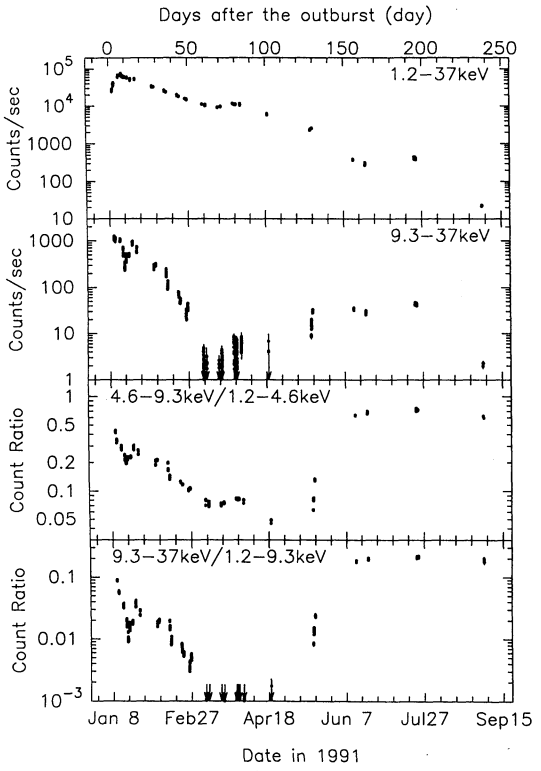

Fig. 2. Time history of the intensities in 1.2–37 keV and 9.3–37 keV, and the hardness-ratios in 4.6–9.3 keV/1.2–4.6 keV and 9.3–37 keV/1.2–9.3 keV. A significant spectral variation is obvious, such that the intensity above 9.3 keV and the hardness ratios do not follow the variations of the total intensity at all. Note that the hardness ratios increased rather suddenly on June 13 and became nearly constant after that, whereas they were largely variable up to May 18 at lower levels. The state transition from the soft state to the hard state seems to have occurred between the two dates.

luminosity reached its peak ($\sim$ 8 Crab) on January 15. The characteristic time scale of the luminosity increase was $\tau \sim 3$ d (where $L \propto e^{t/\tau}$), which is similar to those of A0620−00 ($\sim$ 2.4 d; Elvis et al. 1975) and GS 2000+25 ($\sim$ 3 d; Tsunemi et al. 1989).

(2) Although the light curve after the peak exhibited an exponential decay, which is common to all of the black-hole candidate novae shown together, this is never found in neutron-star novae (for light curves of neutron-star binary novae, see White et al. 1984). The time scale of the luminosity decay ($\sim$ 30 d) is also similar to one another.

(3) GS 1124−68 showed a second luminosity increase at $\sim$ 80 d after the outburst. A0620−00 and GS 2000+25 also showed such a second hump at similar times after the outburst. Furthermore, for GS 1124−68 and A0620−00, the luminosity increased once again $\sim$ 200 d after the outburst.

3.2. *State Transition*

In order to show the long-term spectral variations, the time history of the intensity at 9.3–37 keV and hardness ratios of 4.6–9.3 keV/1.2–4.6 keV and 9.3–37 keV/1.2–9.3 keV are exhibited together with the intensity over the entire energy range (figure 2). From this figure, a significant spectral variation is obvious, such that the intensity above 9.3 keV and the hardness ratios do not follow the variations in the total intensity at all.

In particular, note that the hardness ratios increased rather suddenly on June 13 (157 d after the outburst) and became nearly constant after that, whereas they were irregularly variable at lower levels until May 18 (131 d after the outburst). As shall be shown later (subsection 3.5), the energy spectra up to May 18 are expressed along with the sum of a soft thermal component and a hard power-law component. The variation of the hardness ratios is due to a gradual softening of the soft component and significant and independent variations of the hard component. On the other hand, after June 13 the energy spectra could be approximately expressed using a single power-law function, and the spectral shape became quite stable.

In accordance with the spectral hardening from May to June, the characteristics of the short-term variations also significantly changed. In figure 3, typical short-term intensity variations are shown for the soft (February 21) and hard spectral states (July 22). It is apparent that short-time variations distinguishably increased after the spectral transition. Such intense, "flickering" short-term variations in the hard spectral state are common to Cyg X-1, GX 339−4, and GS 2023+338, and are generally considered to be a common characteristic of black-hole candidates [e.g., Tanaka 1989; Miyamoto, Kitamoto 1989; Miyamoto et al. 1991b; however, it should be noted that the low-mass X-ray binary X1608–522 shows a similar fast time variability as well as power-law like energy spectra in its low-luminosity state (Yoshida et al. 1993).]

The drastic change in the spectral and timing characteristics between 1991 May and June suggests a significant state transition that is reminiscent of the high-low transition of the black-hole candidates Cyg X-1 and GX 339−4. We designate the soft spectral state before the transition simply as "the soft state," and that after the transition as "the hard state" in this paper.

In the soft state up to early February, the intensities of the soft and hard components were almost comparable. The short time variations are relatively large, but still much smaller than those in the hard state (see subsection 3.4 and table 1); the luminosity/spectral dependent Quasi Periodic Oscillations (Dotani 1992) and characteristic time lags between different energy bands (Miyamoto et al. 1993) were observed. These spectral and timing characteristics are similar to those in the "very high state" of GX 339−4 observed in 1988 September (Dotani

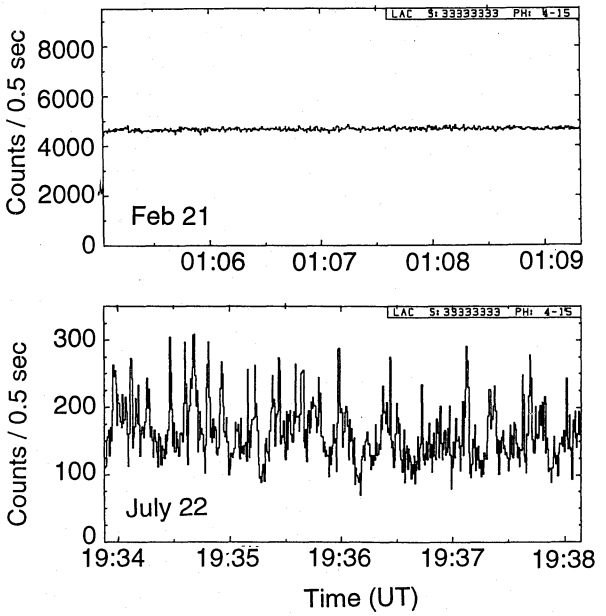

Fig. 3. Representative short-term intensity variations of GS 1124−68 (1 bin = 0.5 s; 2.4–9.0 keV) in the (a) soft spectral state (February 21) and (b) hard spectral state (July 22). The short-term variations are generally small in the soft state (though they are rather significant up to early February; see subsection 3.4 and table 1); on the other hand, the variation is distinguishably strong in the hard state. For quantitative evaluations of short-term variations, see table 1.

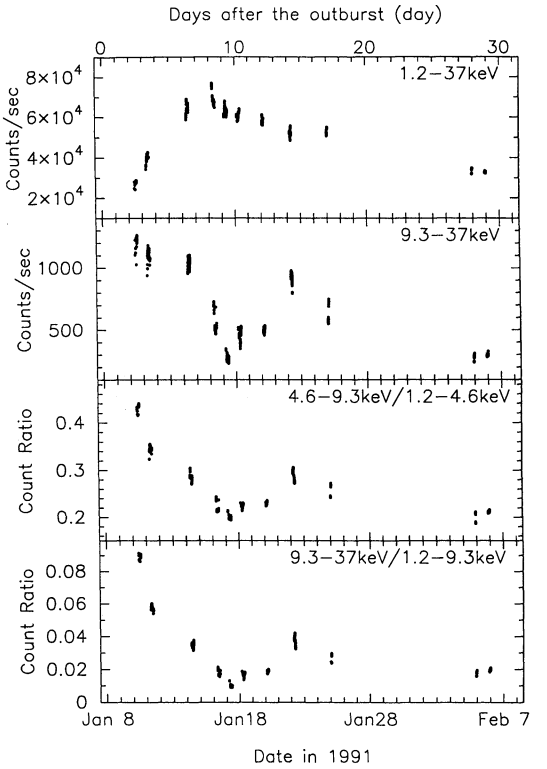

Fig. 4. Time history of the intensities and hardness ratios from the first observation on January 10 to February 6. This is a magnification of the corresponding part of figure 2. From the discovery to the maximum luminosity on January 16, a clear softening of the spectrum was recognized according to the luminosity increase. After the peak, the total luminosity averaged over one day gradually decreased, though the intensity at 9.3–37 keV increased up to January 22. Along with the global luminosity decrease, the intensities and spectral ratios were fluctuating at timescales of less than one day.

1989; Miyamoto et al. 1991a; Dotani 1992; Miyamoto et al. 1993).

3.3. Spectral Variations

In this section, we consider spectral variations of GS 1124−68 for timescales of hours to days. We divide the soft state into four periods, since the characteristics of the energy spectra are rather different in each period.

a) Soft-state 1: from the outburst to the peak

From the first observation by LAC on January 10 to the maximum luminosity on January 16 (8 d after the outburst), the total X-ray intensity progressively increased, while the hard ($\gtrsim$8 keV) flux gradually decreased (figures 4, 5a, 5b). A clear anti-correlation is found between the soft and hard energy range with the spectral "pivot" being at around 8 keV. Note that such a characteristic pivotal spectral evolution is also observed in the growing phase of A0620−00 (Elvis et al. 1975).

b) Soft-state 2: from the peak to early February

During this period, although the total luminosity averaged over one day gradually decreased, the energy spectra were significantly variable, such that the variation was dominant at higher energy. Although the total intensity gradually decreased after the peak on January 16, the hard flux at 9.3–37 keV (as well as the hardness ratio) increased and reached a maximum on January 22 (figure 4). The energy spectra were averaged over each one day; the ratios to that of January 17 are shown in figure 6a and 6b. A gradual decrease over the lower energy range ($\lesssim$6 keV) and significant variations in the higher energy range ($\gtrsim$6 keV) are clearly recognized: an increase from January 17 to 20, then a decrease to February 6, but still higher than the level on January 17.

Although the total luminosity was globally decreasing over longer timescales than one day, there were inten-

Table 1. Energy dependence of fractional variations.*

Date (1991)	Energy range (keV)										
	1.2–37	1.2–2.3	2.3–4.6	4.6–6.9	6.9–9.2	9.2–11.5	11.5–13.8	13.8 –16.1	16.1–18.4	18.4–23	23–37
Jan. 11 ...	6.41±0.02	2.52±0.18	5.65±0.03	11.52±0.05	18.71±0.15	16.16±0.22	18.0±0.4	18.40±0.80	19.0±1.5	23.9±1.5	31.8±3.5
Jan. 22 ...	3.37±0.02	2.19±0.15	2.55±0.03	8.11±0.05	12.52±0.11	16.24±0.23	18.9±0.4	19.1±0.9	21.7±1.6	24.9±1.8	29.0±6.5
Jan. 25 ...	1.41±0.04	1.62±0.43	0.92±0.17	3.68±0.24	6.82±0.58	6.4±1.9	4.7±4.1	11.3±3.7		23±9	
Feb. 5	1.18±0.07	0.83±0.10		3.66±0.32	5.3±1.0	10.2±1.6	8.5±3.7	13.3±4.4		22±10	
Feb. 6	0.83±0.04	0.34±0.19		2.43±0.25	3.82±0.77	4.3±1.8	10.6±1.5	—	—	—	
Feb. 14 ...	1.25±0.04	0.90±0.08		3.92±0.28	6.9±1.1	6.8±3.4	14.8±3.4	—	—	—	
Feb. 21 ...	0.62±0.13	—	—	—	—	—	—	—	—	—	—
Feb. 22 ...	0.60±0.11	—	—	—	—	—	—	—	—	—	—
Feb. 25 ...	0.69±0.21	—	—	—	—	—	—	—	—	—	—
Feb. 27 ...	0.37±0.23	—	—	—	—	—	—	—	—	—	—
Mar. 8	0	—	—	—	—	—	—	—	—	—	—
Mar. 10 ...	0	—	—	—	—	—	—	—	—	—	—
Mar. 12 ...	0.84±0.25	—	—	—	—	—	—	—	—	—	—
Mar. 18 ...	0.73±0.36	—	—	—	—	—	—	—	—	—	—
Mar. 20 ...	0.98±0.28	—	—	—	—	—	—	—	—	—	—
Mar. 28 ...	0.58±0.34	—	—	—	—	—	—	—	—	—	—
Mar. 29 ...	0.23±0.37	—	—	—	—	—	—	—	—	—	—
Mar. 30 ...	0.93±0.28	—	—	—	—	—	—	—	—	—	—
May 17 ...	4.64±0.19	1.6±1.1	5.38±0.31	16.8±0.8		14±7		—	—	—	—
June 13 ...	27.55±0.41	33.1±2.0	28.1±0.8	27.6±1.5	30.1±2.5	17±5		26±13		—	—
July 22 ...	36.0±0.6	34.9±2.7	35.9±0.8	36.5±1.2	35.4±2.1	40.6±2.0		46±6		—	—
July 23 ...	36.6±0.4	38.7±1.9	35.6±0.6	35.9±0.9	35.6±1.5	36.0±1.7		36±6		—	—

* Fractional variations are defined as F.V. $= 1/(N-1)\Sigma_{i=1}^{N}\left\{(x_i-\bar{x})^2-\bar{x}\right\}/(\bar{x}-b)$, where x_i is the counts in the i-th bin, $\bar{x}$ is the average counts over N-bins, and b is the background. We took the binwidth = 8 ms, $N = 16384$, and thus calculated Fractional Variations over the timescale 16 ms to 128 s. Fractional Variations were calculated for each 128 s segment, then ensemble average was obtained.

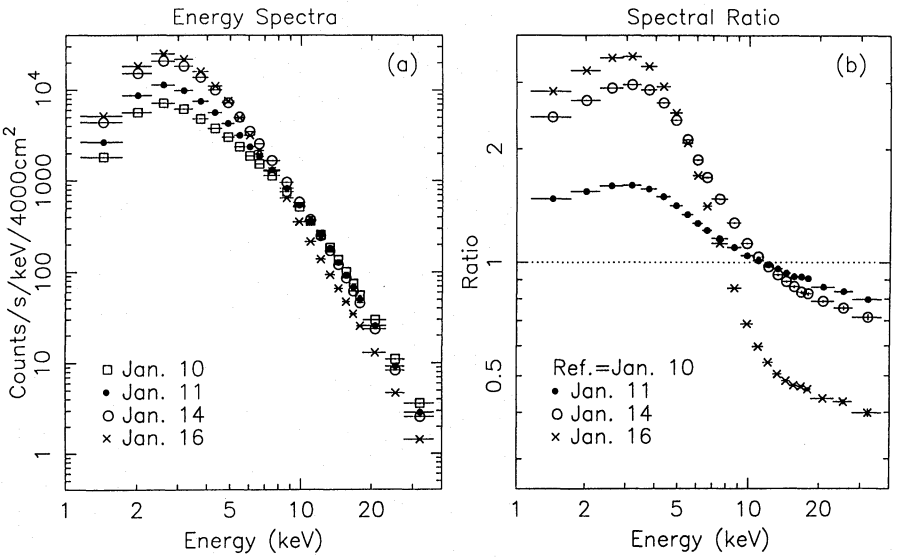

Fig. 5. (a) Energy spectra of GS 1124−68 from the first observation with LAC (January 10) to the maximum luminosity (January 16). (b) The ratios of these energy spectra to that on January 10. As the total luminosity increases, the energy spectra show pivotal variations, such that the hard flux decreases while the soft flux increases, with the spectral pivot being at around 8 keV.

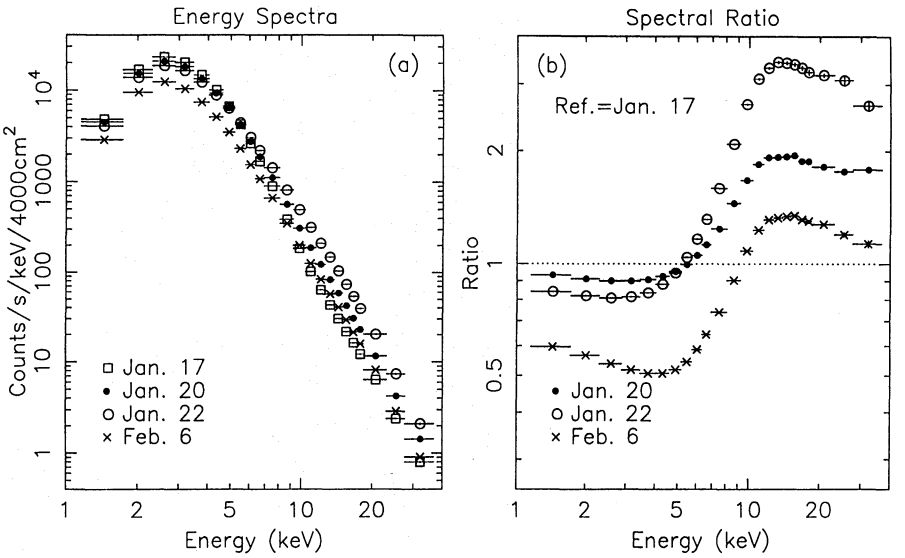

Fig. 6. (a) Energy spectra from January 17 to February 6, each averaged over one day. (b) The ratios of these energy spectra to that on January 17. A gradual decrease in the soft energy range ($\lesssim$6 keV) and significant variations in the hard energy range ($\gtrsim$6 keV) are recognized.

sity fluctuations and accompanying spectral variations with timescales in the range of several tens of minutes to hours. Examples of particularly notable variations (those on January 17 and January 18) are shown in figures 7a and 7b. Also note that on these timescales, the hard X-rays are more significantly variable than the soft X-rays.

c) Soft-state 3: from the mid-February to April

During this period, the total luminosity constantly decayed, except for a characteristic luminosity increase on March 28, 79 d after the outburst (corresponding to the "hump" in the light curve; see figures 1 and 2). The luminosity decay is more significant at higher energies ($\gtrsim$10 keV); the high-energy flux above $\sim$ 10 keV nearly

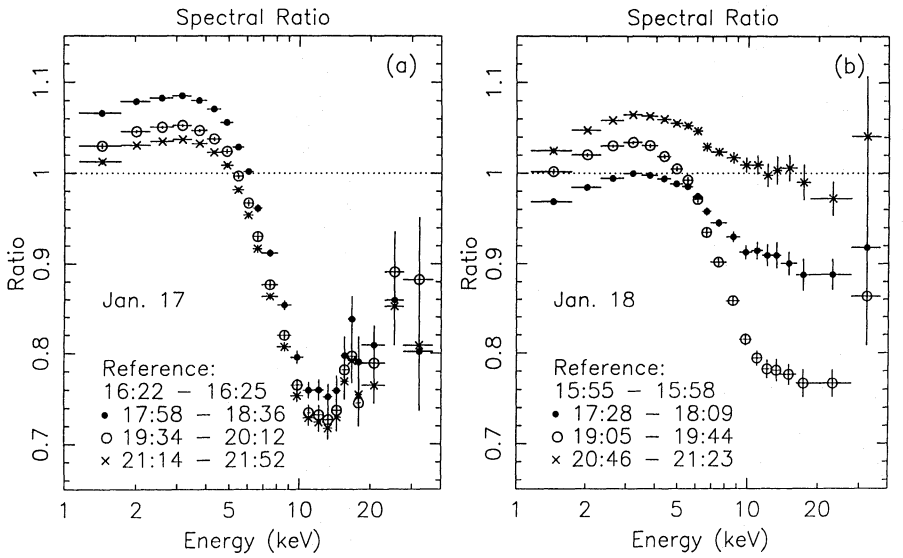

Fig. 7. (a) Ratios of the energy spectra with short (< 1 h) exposures on January 17. The soft ($\lesssim$5 keV) intensity increased from 16:25 to 17:58, whereas the hard intensity significantly decreased. Then, the soft intensity gradually decreased and the hard intensity remained nearly at the same level. (b) Ratios of the energy spectra with short exposures on January 18. The soft ($\lesssim$5 keV) intensity firstly decreased (from 15:58 to 17:28) then gradually increased (from 18:09 to 20:46), whereas the hard flux seems to vary independently.

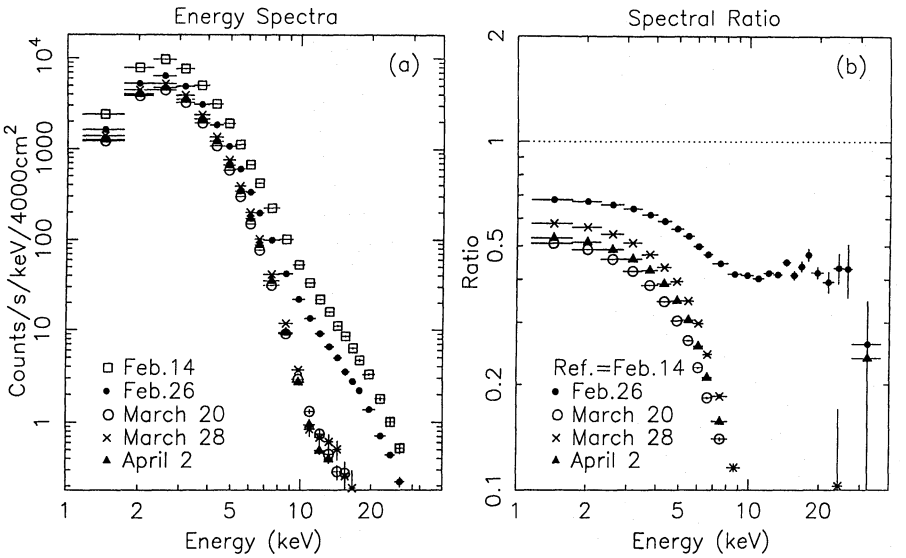

Fig. 8. (a) Energy spectra of GS 1124−68 from February 14 to April 2, and (b) those spectral ratios to that on February 14. A temporary luminosity increase was found on March 28. Note that the intensity decay was more significant at higher energies, and the hard component above $\sim$ 10 keV was hardly detected in late March and April. The energy spectra in February showed a convex feature at around $\sim$ 8 keV, implying that the energy spectrum comprise soft and hard components which are, respectively, dominant below and above that energy.

disappeared in late March and April (figures 8a and 8b). Significant intensity variations on timescales shorter than hours are not recognized.

Some energy spectra during this period (and the next period) showed a convex feature at 8–10 keV (figure 8a), suggesting that they comprised soft and hard components, which are dominant, respectively, below and above $\sim$ 9 keV.

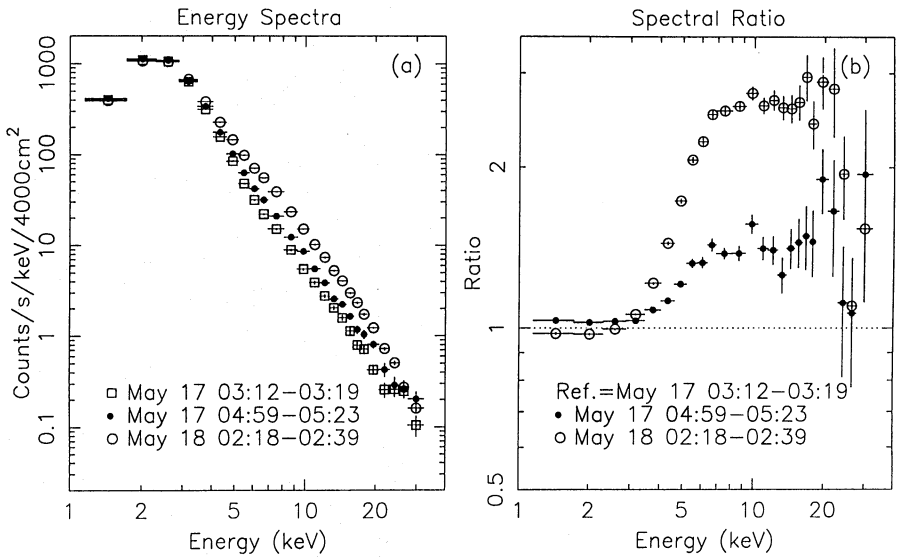

Fig. 9. (a) Energy spectra taken on May 17 and 18 with short exposures, and (b) those ratios to that taken at 03:12–03:19 on May 17. The soft ($\lesssim$6 keV) luminosity has steadily decreased from the previous observation in April, though the hard luminosity conversely and significantly increased (compare with figure 8). Within the two-day observation, the hard flux ($\gtrsim$6 keV) increased by as much as a factor of $\sim$ 3, whereas the soft flux only slightly decreased.

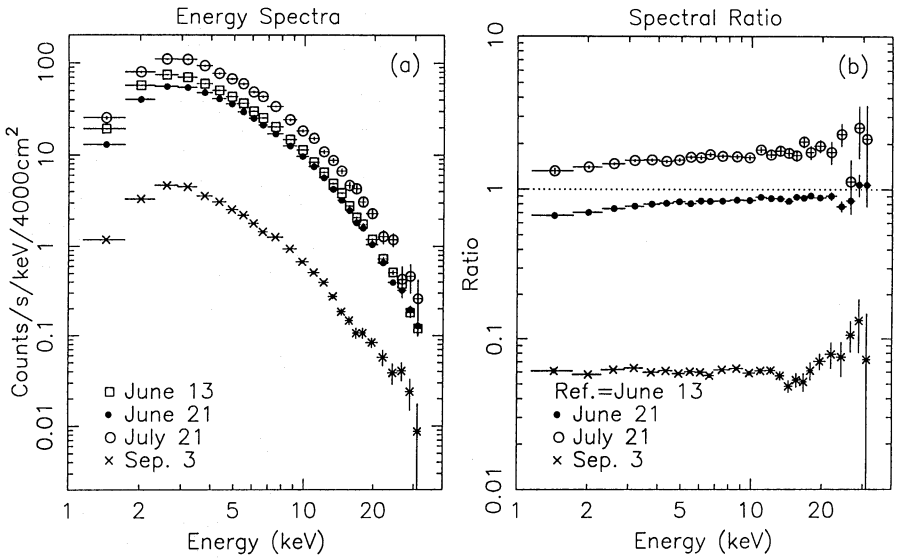

Fig. 10. (a) Energy spectra in the hard state from June 13 to September 3 (last detection) and (b) the spectral ratio compared to that on June 13. In the hard state, the energy spectra became much harder than those in the soft state (compare with figure 9a). The luminosity gradually decayed (except for a temporary increase on July 21–23), while maintaining almost the same spectral shape throughout the hard state. Note that the spectrum on July 21 corresponds to the temporary luminosity increase.

d) Soft-state 4: May 17 and 18 (129 and 130 d after the outburst)

Although the soft ($\lesssim$6 keV) luminosity has steadily decreased from the previous observation in April, the hard luminosity, conversely, increased (figure 9a). Within the two days of observations, the soft intensity decayed very slightly; on the other hand, the hard component gradually increased by a factor of three (figures 9a, b).

e) Hard state: from June to September

After June 13 (156 d after the outburst) in the hard state, the energy spectra became much harder (compare

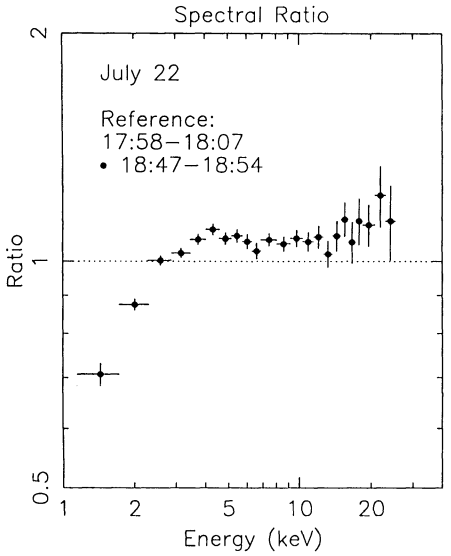

Fig. 11. An example of the short-term spectral variations in the hard state. The spectral ratio between those taken at 18:47–18:54 and 17:58–18:07 on July 22 is displayed. A significant soft flux variation ($\lesssim$3 keV) can be recognized. Such soft X-ray variations on short timescales were often observed in the hard state, but never found in the soft state.

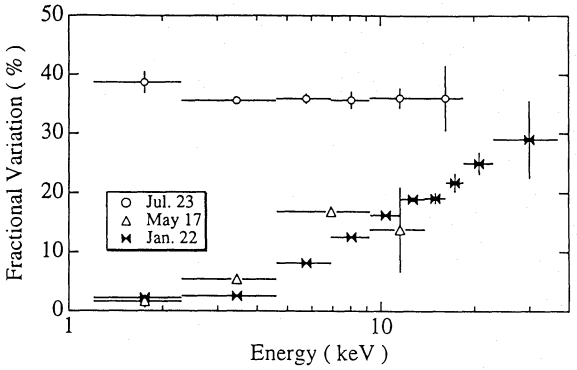

Fig. 12. Energy dependence of Fractional Variations (F.V.) for the soft (January 22 and May 17) and hard (July 23) states on timescale of 16 ms to 128 s. In the soft state, F.V. are clearly larger at higher energies; on the other hand, F.V. become nearly energy independent in the hard state at a much higher level than in the soft state.

figures 9a and 10a). The total luminosity gradually decayed (except for the temporary increase on July 21–23), while holding a nearly constant spectral shape up to the last detection on September 3 (figures 10a, b). A variation in the soft flux ($\lesssim$3 keV) on timescales of several tens of minutes to hours, which was never observed in the soft state, was often observed during the hard state (figure 11). The spectral shape above $\sim$ 3 keV was very stable within one day, although the short-term intensity variations were remarkably significant (figure 3).

3.4. Short-Term Spectral Variations

In order to quantitatively study spectral variations on timescales shorter than several hundred seconds, we calculated the fractional variations for each observation period and for different energy bands. The fractional variations (F.V.) are defined here as

$$\text{F.V.} = \frac{1}{N-1}\sum_{i=1}^{N}\{(x_i-\bar{x})^2-\bar{x}\}^{1/2}\Big/(\bar{x}-b), \quad (1)$$

where x_i is the intensity of the i-th timing bin, b is the background, and N is the number of bins. We took a bin width of 8 ms and N = 16384, and thus studied variations of between 16 ms and 128 s. For each MPC3 observation (time resolution of 8 ms), the data were divided into 16384 bin (= 128 s) segments, and the F.V. were calculated for each segment; the ensemble average was then obtained. A calculation was made for the total energy band (1.2–37 keV) for all of the data, as well as for smaller energy bands for those data having sufficient statistics. All of the results are tabulated in table 1, and typical F.V. in the soft (January 22 and May 17) and hard states (July 23) as a function of energy are displayed in figure 12.

From table 1 and figure 12, it is obvious that F.V. in the total energy range dramatically increased after the transition to the hard state (this is readily anticipated in figure 3). In the soft state, the F.V. are relatively large when the high-energy component ($\gtrsim$7 keV) is strong; although F.V. gradually decreased from January to March as the hard flux decreased (see subsection 3.3b and c), it rather suddenly increased in May in accordance with an increase of the hard flux (see subsection 3.3d). Furthermore, F.V. were larger for higher energies in the soft state when there were significant variations. These facts indicate that the short-term variations in the soft state are mainly associated with the high-energy spectral component. It is also important that the QPO was observed only up to middle of February (Dotani 1992), when the intensity of the hard X-rays was rather strong. This suggests that the hard component is playing a major role in the QPO phenomena. On the other hand, in the hard state, no apparent energy dependence was found (table 1, figure 12). This seems to be related to the stability of the hard-state energy spectra, such that the spectral shape above $\sim$ 3 keV hardly changed on any timescale longer than several tens of minutes (subsection 3.3e).

These characteristics of the spectral variations of GS 1124−68 both in the soft and hard state are com-

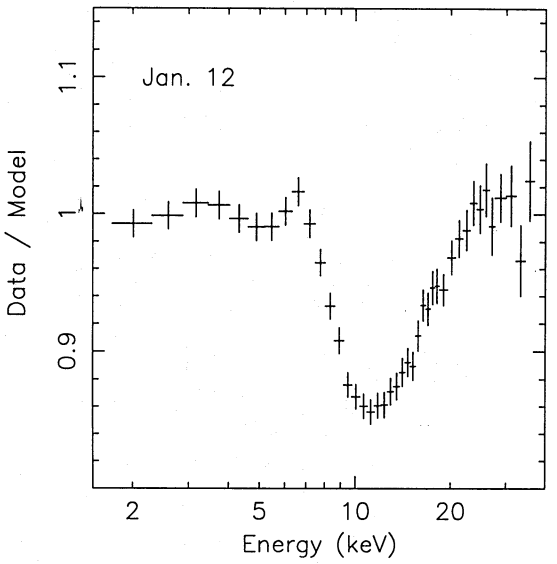

Fig. 13. Spectral ratio of the energy spectrum in the soft state (January 12) to the model function, which is a sum of the multicolor disk model (soft component) and a power-law function (hard component). A broad absorption feature above $\sim$ 7 keV can be clearly seen. The same structure is found in both the soft and hard states, whenever there is a significant hard flux above $\sim$ 7 keV.

mon to black-hole candidates LMC X-1 (soft state), GS 2000+25 (soft state), Cyg X-1 (hard state), GS 2023+338 (hard state), and GX 339−4 (soft and hard states) (Ebisawa 1991; Miyamoto et al. 1991a, b; Inoue 1992).

3.5. *Spectral Fitting*

The spectral variations of GS 1124−68 illustrated in the previous two sections suggest that the soft-state spectrum comprises two components, which are respectively dominant in the soft ($\lesssim$7 keV) and hard ($\gtrsim$7 keV) energy bands. Also, in the hard state, the spectral variation at low energies (figure 11) indicates the existence of a soft excess component in addition to the main hard component. Hence, we adopted a two-component model and tried to fit both the soft- and hard-state energy spectra with the same model. We adopted the multicolor disk model (Mitsuda et al. 1984; Makishima et al. 1986) for the soft component, which approximates the emission from an optically thick accretion disk, and a power-law function for the hard component. The choice of the model is rather arbitrary [actually, the hard component can also be fitted using the Comptonized blackbody model by Nishimura et al. (1986)]; our main purpose is to describe the energy spectra quantitatively, so that we can discuss and compare different outburst phases as well as other sources (see section 4).

As a result of trial fitting with the multicolor disk + power-law model, we found that both the soft- and hard-state energy spectra show a significant local absorption structure above $\sim$ 7 keV whenever there is a significant amount of hard X-rays (figure 13). The absorption structure always starts at $\sim$ 7 keV, which suggests that the structure is due to iron K-absorption. The observed absorption structure, however, cannot be fitted with a simple iron K-edge absorption, because the observed structure is much broader or shallower than the iron K-edge structure. Similar broad absorption features have been observed from black-hole candidates such as Cyg X-1 (Inoue 1989; Tanaka 1990; Done et al. 1992), GS 2023+338 (Inoue 1989; Yoshida 1990; Tanaka 1990), LMC X-1 (Ebisawa 1991), GS 2000+25 (Takizawa 1991; Ebisawa 1991), and GX 339−4 (Ueda et al. 1994), the low mass X-ray binary X1608−522 (Yoshida et al. 1993), and several Seyfert 1 galaxies (e.g., Matsuoka et al. 1990; Piro et al. 1990; Pounds et al. 1990; see also Inoue 1989). These broad absorption structures are widely explained in terms of the reflection of X-rays by optically thick accretion disks around the central compact objects (e.g., Guilbert, Rees 1988; Lightman, White 1988). Partial absorption models are also proposed (e.g., Matsuoka et al. 1990; Yoshida et al. 1993).

Although many reflection or partial absorption models have been calculated and proposed, in order to fit the observed energy spectra, we introduce a simple mathematical model which modifies the iron K-absorption structure. When a photon spectrum undergoes iron K-absorption, the spectrum is reduced by a factor of $\exp[-\sigma_{\rm Fe}(E, E_{\rm edge})\, N_{\rm Fe}]$, where $\sigma_{\rm Fe}(E, E_{\rm edge})$ is the iron cross section and $N_{\rm Fe}$ is the iron column density. To model the observed broad absorption feature, instead, we introduced a fictitious cross section $\sigma'(E, E_{\rm edge}, E_{\rm W})$, such that

$$\sigma'(E, E_{\rm edge}, E_{\rm W}) = \begin{cases} 0 & (E < E_{\rm edge}) \\ \sigma_{\rm Fe}(E, E_{\rm edge}) \left[1 - \exp\left(-\dfrac{E - E_{\rm edge}}{E_{\rm W}}\right)\right] & (E > E_{\rm edge}), \end{cases} \quad (2)$$

where $E_{\rm edge}$ is the K-edge energy and $E_{\rm W}$ describes the artificial edge broadening (or smearing) effect. We ignored the L-shell absorption at $E < E_{\rm edge}$. For the iron cross section, that by McMaster et al. (1970) was adopted.

Since the broad edge structure is conspicuous when the hard flux above $\sim$ 7 keV is strong, we applied the attenuation factor $\exp[-\sigma'(E, E_{\rm edge}, E_{\rm W})\, N_{\rm Fe}]$, which we may call the "smeared edge model," only to the power-law component. After all, the spectral model that we

adopted is

$$\exp\left[-\sigma_{\rm abs}(E)N_{\rm H}\right]\left\{f(E, r_{\rm in}\sqrt{\cos\theta}/d, T_{\rm in}) + A\,E^{-\alpha}\exp\left[-\sigma'(E, E_{\rm edge}, E_{\rm W})\,N_{\rm Fe}\right]\right\}, \quad (3)$$

where $\sigma_{\rm abs}(E)$ is the cross section for interstellar absorption, for which we used that by Morison and McCammon (1983), $f(E, r_{\rm in}\sqrt{\cos\theta}/d, T_{\rm in})$ is the multicolor disk model, which is a function of the innermost temperature $T_{\rm in}$ and the projected disk radius $r_{\rm in}\sqrt{\cos\theta}$ at a given radius d, and A is the normalization for the power-law component. Since there is a strong coupling between $E_{\rm W}$ and $N_{\rm Fe}$ (Ebisawa 1991), we fixed $E_{\rm W}$ to 10 keV. However, the results were hardly affected by the choice of $E_{\rm W}$. At last, the free parameters of the model fitting are $N_{\rm H}, T_{\rm in}, r_{\rm in}\sqrt{\cos\theta}$ (at a given radius d), $A, \alpha, E_{\rm edge}$, and $N_{\rm Fe}$. The same spectral model was successfully applied for both the soft- and hard-energy spectra of the black-hole candidates Cyg X-1, LMC X-3, LMC X-1, GX 339−4, and GS 2000+25 observed with Ginga (Ebisawa 1991).

For overall the observational periods, we typically extracted energy spectra by integrating for $\sim$ 30 min; spectral fitting were carried out for those spectra that apparently varied from others. For each energy bin, we introduced systematic errors which were 1% of the observed counts. In March and April in the soft state, hard X-rays above $\sim$ 7 keV were so weak that the photon index of the hard component was hardly constrained, and no broad absorption structure could be recognized. In this case, we determined the results by fixing the photon-index to 2.6 (the average of those before March) and eliminated the smeared-edge model. On September 3 in the hard state, the smeared-edge model was not applied, since the intensity was low and no broad absorption feature could be recognized. For several spectra for which the $N_{\rm H}$ values became too small and were not determined from the fitting, the values were fixed at $10^{21.2}$ cm^{-2}, which is the average of the others.

The best-fit parameters of the fitting are tabulated in table 2, and some of the fitted spectra are displayed in figure 14. The model can fit energy spectra both in the soft and hard states quite well, except for those during March and April, in which the hard component was very weak. The fit could be better (reduced $\chi^2 \lesssim 2.65$) if we allow the power-law index of the hard component to be free, and introduce the smeared-edge model and an additional emission line at 6.7 keV. However, it would be more natural to consider that the multicolor disk model breaks down when the hard component is very weak and the "bare" soft component emerges. Even so, deviations between the multicolor disk model and the data are at most $\sim$ 5% for each spectral bin (with Poisson errors much less than 1%) and, therefore, the multicolor disk model parameters are still useful for comparing the energy spectra at different periods with each other and with the energy spectra of other sources (for a discussion concerning the accretion-disk spectra, see subsection 4.3).

The time variation of the best-fit values for the major model parameters is shown in figure 15. We summarize below the noticeable results of the spectral fitting:
(1) From the outburst to the peak, the ratio of the soft component and the hard component was approximately even. Corresponding to a softening of the energy spectra (figures 4, 5), the power-law component steepened and the temperature of the soft component increased.
(2) Between the peak and the end of the soft state (May 18), the soft component accounted for most of the X-ray luminosity. During this period, the soft component decreased by about one order of magnitude, accompanying a remarkable temperature decrease from 0.98 to 0.5 keV. The temperatures are lower than the typical values for bright low-mass X-ray binaries ($\sim$ 1.4 keV; e.g., Mitsuda et al. 1984), but comparable to those for other black-hole candidates (e.g., Makishima et al. 1986; Ebisawa et al. 1989; Treves et al. 1990; Ebisawa 1991; Ebisawa et al. 1993). The radius of the disk, on the other hand, did not show any systematic variations, but, rather, stayed within a narrow range of 9–15 km (at 1 kpc). At the temporary luminosity increase at the end of March, although the disk temperature increased, the radius did not change.
(3) The photon-index of the power-law component clearly changed between the soft and hard states. In the soft state, it was within 2.2–2.7, but in the hard state, it became $\sim$ 1.6.
(4) After the transition to the hard state, the soft-component luminosity considerably decreased, and the hard component became the major component. Subsequently, the hard component decreased with the photon-index constant at $\sim$ 1.6.

4. Discussion

In this section, based on the observational results presented so far, we discuss the outburst and spectral transition mechanism, the origin of the soft and hard components, and the origin of the broad absorption structure.

4.1. Long-Term Luminosity Evolution

After the maximum light on the January 16th (8 d after the outburst), the X-ray flux of GS 1124−68 decayed with an e-folding time of $\sim$ 30 d. The second and third "humps" were, respectively, detected $\sim$ 80 d and $\sim$ 200 d after the outburst.

The mass accretion rate after the maximum, assumed to be simply proportional to the X-ray intensity, may be expressed as $\dot{M}(t) \propto \exp(-t/\tau)$, where τ is $\sim$ 30 d. Integrating this relation, we obtain $\dot{M}(t) = [M(\infty) -$

Table 2. Results of spectral fitting.

Time (UT; 1991)	$R_{\rm in}\sqrt{\cos\theta}$ (km at 1 kpc)	$T_{\rm in}$ (keV)	Photon index	Soft flux* (10^{-9}erg s^{-1}cm^2)	Hard flux†	log $N_{\rm Fe}$ (cm^{-2})	Edge energy (keV)	log $N_{\rm H}$ (cm^{-2})	Reduced χ^2 (d.o.f)
1/10 19:44–00:21	33^{+24}_{-11}	$0.40^{+0.05}_{-0.03}$	2.24±0.01	60^{+230}_{-40}	66.7±3.0	19.55±0.04	7.42±0.17	$21.7^{+0.2}_{-0.3}$	1.00 (39)
1/11 00:55–01:09	60^{+28}_{-17}	$0.35^{+0.03}_{-0.02}$	2.25±0.01	120±70	71.1±2.8	19.52±0.04	7.56±0.18	$21.9^{+0.1}_{-0.2}$	1.51 (39)
1/11 20:26–20:44	$8.5^{+5.0}_{-1.9}$	$0.65^{+0.09}_{-0.08}$	$2.50^{+0.01}_{-0.02}$	30^{+90}_{-20}	85.2±4.0	$19.67^{+0.03}_{-0.06}$	7.45±0.17	21.6±0.1	0.51 (39)
1/14 19:48–20:04	$7.5^{+0.8}_{-0.6}$	0.92±0.04	$2.65^{+0.03}_{-0.04}$	87±23	95±12	$19.81^{+0.05}_{-0.04}$	7.66±0.16	21.7±0.1	0.98 (39)
1/14 20:48–21:11	$7.4^{+0.6}_{-0.5}$	0.96±0.04	$2.61^{+0.03}_{-0.04}$	102±20	92±12	19.8 ±0.1	7.92±0.18	21.6±0.1	0.96 (39)
1/14 22:39–23:24	$8.1^{+0.8}_{-0.6}$	0.92±0.04	2.62±0.03	99±25	96±11	19.8 ±0.4	7.86±0.17	21.6±0.1	1.25 (39)
1/16 18:46–19:06	$9.5^{+0.5}_{-0.4}$	0.95±0.03	2.81±0.05	157±24	85±14	$19.9\ ^{+0.1}_{-0.4}$	7.84±0.15	21.7±0.1	1.06 (39)
1/16 20:02–20:15	$11.1^{+0.6}_{-0.4}$	0.92±0.02	$2.64^{+0.07}_{-0.06}$	194±26	52±14	$19.9\ ^{+0.1}_{-0.4}$	7.69±0.17	$21.4^{+0.1}_{-0.2}$	1.59 (37)
1/16 21:45–22:20	11.1±0.5	0.92±0.02	2.67±0.05	190±24	52±10	19.9 ±0.1	7.72±0.15	21.5±0.1	1.36 (34)
1/16 23:23–23:26	$10.1^{+0.5}_{-0.4}$	0.94±0.02	$2.73^{+0.07}_{-0.08}$	169±24	59±16	$19.9\ ^{+0.1}_{-0.4}$	7.58±0.23	$21.5^{+0.1}_{-0.2}$	1.02 (36)
1/17 16:22–16:25	9.9±0.4	0.96±0.02	$2.74^{+0.09}_{-0.10}$	178±20	40±14	$20.0\ ^{+0.1}_{-0.3}$	7.56±0.19	$21.3^{+0.2}_{-0.3}$	1.16 (27)
1/17 17:58–18:36	11.0±0.4	0.952±0.013	$2.60^{+0.07}_{-0.08}$	215±18	27±8	20.1 ±0.1	7.41±0.16	$21.1^{+0.2}_{-0.3}$	0.71 (33)
1/17 19:34–20:12	10.7±0.3	$0.966^{+0.009}_{-0.012}$	$2.42^{+0.07}_{-0.09}$	215±16	20±7	$19.96^{+0.01}_{-0.07}$	7.43±0.25	< 20.9	0.73 (39)
1/17 21:14–21:52	10.8±0.3	0.957±0.013	$2.53^{+0.07}_{-0.08}$	210±17	23±7	$20.01^{+0.04}_{-0.11}$	7.36±0.20	$21.0^{+0.2}_{-0.4}$	0.51 (39)
1/18 15:55–15:58	9.1±0.4	0.97±0.02	2.64±0.08	155±21	50±23	$18.91^{+0.04}_{-0.08}$	7.66±0.22	$21.2^{+0.2}_{-0.5}$	0.87 (39)
1/18 17:28–18:09	$9.2^{+0.4}_{-0.3}$	0.975±0.018	$2.59^{+0.05}_{-0.06}$	166±18	41±9	19.9 ±0.1	7.70±0.18	$21.0^{+0.2}_{-0.4}$	0.87 (39)
1/18 19:05–19:44	9.6±0.3	$0.981^{+0.013}_{-0.016}$	2.54±0.06	183±16	33±7	19.9 ±0.1	7.74±0.19	< 21.0	1.15 (39)
1/18 20:48–21:23	$9.5^{+0.4}_{-0.3}$	0.972±0.018	2.60±0.05	173±19	46±9	19.9 ±0.1	7.78±0.17	$21.2^{+0.2}_{-0.3}$	0.87 (39)
1/20 14:58–15:33	9.2±0.4	0.969±0.019	$2.59^{+0.05}_{-0.06}$	162±19	44.6±9.5	19.9 ±0.1	7.69±0.18	$21.1^{+0.2}_{-0.5}$	1.02 (39)
1/20 16:30–17:12	$9.0^{+0.4}_{-0.3}$	0.974±0.019	2.57±0.05	158±18	44±9	19.9 ±0.1	7.78±0.18	$21.0^{+0.2}_{-0.5}$	0.77 (39)
1/22 20:36–20:42	$7.5^{+0.6}_{-0.4}$	$0.95^{+0.03}_{-0.04}$	2.61±0.04	99±17	79±12	$19.8\ ^{+0.04}_{-0.10}$	7.62±0.20	$21.5^{+0.10}_{-0.2}$	0.96 (39)
2/ 6 07:10–08:55	9.1±0.5	0.87±0.02	2.68±0.04	101±15	35±5	$19.90^{+0.03}_{-0.04}$	7.56±0.13	$21.4^{+0.1}_{-0.2}$	1.25 (39)
2/13 05:06–05:22	$9.1^{+0.6}_{-0.5}$	0.81±0.021	2.65±0.04	77±13	25.1±3.5	$19.99^{+0.03}_{-0.04}$	7.66±0.13	21.3±0.2	1.10 (35)
2/13 06:40–06:56	$10.6^{+0.6}_{-0.5}$	$0.784^{+0.016}_{-0.017}$	2.54±0.04	91±13	17.7±2.7	20.02±0.02	7.56±0.12	$21.1^{+0.2}_{-0.4}$	0.96 (36)
2/13 08:14–08:33	$10.5^{+0.6}_{-0.5}$	$0.795^{+0.016}_{-0.015}$	$2.48^{+0.04}_{-0.05}$	95±13	15.4±2.5	20.02±0.02	7.6 ±0.14	$20.9^{+0.3}_{-0.8}$	1.27 (39)
2/14 04:36–04:52	$11.7^{+0.7}_{-0.6}$	0.757±0.015	2.61±0.08	97±13	11.0±3.1	$20.12^{+0.02}_{-0.04}$	7.31±0.14	$20.9^{+0.3}_{-0.8}$	1.77 (27)
2/14 05:30–05:33	$12.5^{+0.8}_{-0.7}$	0.74±0.017	$2.64^{+0.11}_{-0.12}$	101±16	11.9±4.5	$20.14^{+0.04}_{-0.07}$	7.19±0.18	$21.2^{+0.2}_{-0.4}$	0.59 (27)
2/20 23:31–23:36	12.1±0.6	0.74±0.013	$2.52^{+0.07}_{-0.08}$	94±12	7.6±2.1	$20.07^{+0.03}_{-0.09}$	7.17±0.16	$21.2^{+0.2}_{-0.3}$	0.84 (35)
2/21 00:23–00:29	$12.1^{+0.7}_{-0.6}$	$0.735^{+0.013}_{-0.014}$	2.58±0.08	93±12	8.3±2.3	$20.10^{+0.03}_{-0.06}$	7.21±0.15	$21.2^{+0.2}_{-0.3}$	0.93 (34)

Table 2. (Continued)

Time (UT; 1991)	$R_{\rm in}\sqrt{\cos\theta}$ (km at 1 kpc)	$T_{\rm in}$ (keV)	Photon index	Soft flux* (10^{-9}erg s^{-1}cm^2)	Hard flux† (10^{-9}erg s^{-1}cm^2)	log $N_{\rm Fe}$ (cm^{-2})	Edge energy (keV)	log $N_{\rm H}$ (cm^{-2})	Reduced χ^2 (d.o.f)
3/ 8 18:04–18:21	11.12±0.11	0.707±0.002	2.6 (fixed)	66.7±1.6	0.5 ±0.014	—	—	21.2 (fixed)	12.35 (24)
3/10 16:56–17:16	11.91±0.13	0.678±0.002	2.6 (fixed)	64.7±1.6	0.383±0.020	—	—	21.2 (fixed)	9.48 (24)
3/20 12:56–13:16	10.66±0.11	0.702±0.002	2.6 (fixed)	59.6±1.3	0.264±0.012	—	—	21.2 (fixed)	15.41 (24)
3/28 09:37–09:42	11.17±0.12	0.716±0.002	2.6 (fixed)	70.9±1.8	0.272±0.026	—	—	21.2 (fixed)	7.36 (24)
3/29 05:54–06:05	10.8±0.1	0.72 ±0.002	2.6 (fixed)	68 ±1.3	0.154±0.014	—	—	21.2 (fixed)	10.08 (18)
3/30 08:36–08:53	9.79±0.09	0.733±0.002	2.6 (fixed)	59.8±1.3	0.123±0.012	—	—	21.2 (fixed)	13.77 (18)
4/ 2 05:04–05:29	10.63±0.10	0.716±0.002	2.6 (fixed)	64.2±1.3	0.162±0.010	—	—	21.2 (fixed)	12.21 (18)
4/19 21:06–21:19	15.7±0.3	0.552±0.003	2.6 (fixed)	49.4±2.3	0.529±0.058	—	—	21.2 (fixed)	3.26 (18)
5/17 03:12–03:19	$14.0\pm^{1.1}_{0.9}$	0.488±0.009	2.28±0.10	23.9±4.0	0.92±0.31	20.0 ±0.1	7.17±0.23	$21.3\pm^{0.2}_{0.3}$	0.59 (27)
5/17 04:34–04:56	$13.0\pm^{0.9}_{0.8}$	0.502±0.008	2.19±0.06	23.3±3.7	1.17±0.30	$20.03\pm^{0.04}_{0.05}$	7.13±0.14	$21.0\pm^{0.2}_{0.7}$	1.25 (27)
5/17 07:49–08:09	$13.0\pm^{0.9}_{0.8}$	0.502±0.008	2.24±0.05	23.1±3.6	1.37±0.25	$20.00\pm^{0.03}_{0.05}$	7.41±0.12	$21.3\pm^{0.2}_{0.3}$	0.78 (24)
5/18 02:18–02:39	$11.2\pm^{1.0}_{0.2}$	$0.511\pm^{0.003}_{0.011}$	2.24±0.03	18.5±3.4	2.36±0.30	$19.96\pm^{0.02}_{0.04}$	7.24±0.11	< 20.3	1.2 (32)
5/18 03:52–04:16	$11.9\pm^{1.2}_{0.4}$	$0.499\pm^{0.005}_{0.011}$	2.31±0.03	18.8±3.7	2.58±0.25	$19.93\pm^{0.02}_{0.04}$	7.27±0.11	< 20.9	0.74 (27)
5/18 05:25–05:51	$12.1\pm^{1.1}_{0.4}$	$0.497\pm^{0.004}_{0.011}$	2.19±0.06	19.4±3.6	2.67±0.60	$19.98\pm^{0.02}_{0.04}$	7.34±0.10	< 20.9	1.05 (27)
6/13 13:20–16:46	$4.0\pm^{1.3}_{0.7}$	0.36±0.03	1.64±0.02	$0.6\pm^{0.8}_{0.3}$	1.14±0.04	19.4 ±0.1	7.3±0.3	21.2 (fixed)	0.99 (28)
6/21 11:04–13:44	$4.2\pm^{3.4}_{1.0}$	0.32±0.05	1.64±0.02	$0.4\pm^{1.9}_{0.3}$	0.93±0.04	$19.15\pm^{0.02}_{0.23}$	6.9±0.5	21.2 (fixed)	1.33 (28)
7/21 21:53–22:12	$2.0\pm^{1.0}_{0.4}$	0.44±0.05	1.53±0.02	$0.3\pm^{0.8}_{0.2}$	1.41±0.06	19.4 ±0.1	7.2±0.4	21.2 (fixed)	0.94 (28)
7/22 17:58–18:07	$6.7\pm^{2.5}_{1.2}$	0.33±0.03	1.54±0.03	$1.2\pm^{1.8}_{0.7}$	1.33±0.07	$19.3\pm^{0.2}_{0.3}$	7.3±0.8	21.2 (fixed)	0.66 (28)
7/22 18:47–18:54	$1.3\pm^{1.2}_{0.2}$	0.51±0.11	1.49±0.05	$0.2\pm^{1.8}_{0.13}$	1.43±0.14	$19.5\pm^{0.2}_{0.3}$	7.4±0.7	21.2 (fixed)	0.96 (28)
7/23 17:07–17:20	$4.0\pm^{3.9}_{0.7}$	0.33±0.06	1.57±0.03	$0.4\pm^{2.7}_{0.27}$	1.48±0.07	$19.1\pm^{0.2}_{0.3}$	6.7±0.6	21.2 (fixed)	0.85 (28)
7/23 17:54–18:02	$2.5\pm^{2.1}_{0.5}$	0.40±0.07	1.57±0.03	$0.3\pm^{1.0}_{0.2}$	1.48±0.07	$19.1\pm^{0.2}_{0.3}$	6.7±0.6	21.2 (fixed)	0.85 (28)
9/ 3 03:55–13:21	$2.5\pm^{15.0}_{0.3}$	0.26±0.10	$1.84\pm^{0.03}_{0.04}$	$0.06\pm^{10}_{0.05}$	0.07±0.04	—	—	21.2 (fixed)	1.53 (26)

* The soft flux is the bolometric flux calculated with the formula $2\sigma(r_{\rm in}\sqrt{\cos\theta}/d)^2\ {T_{\rm in}}^2$.
† The hard flux is calculated for 2–20 keV.

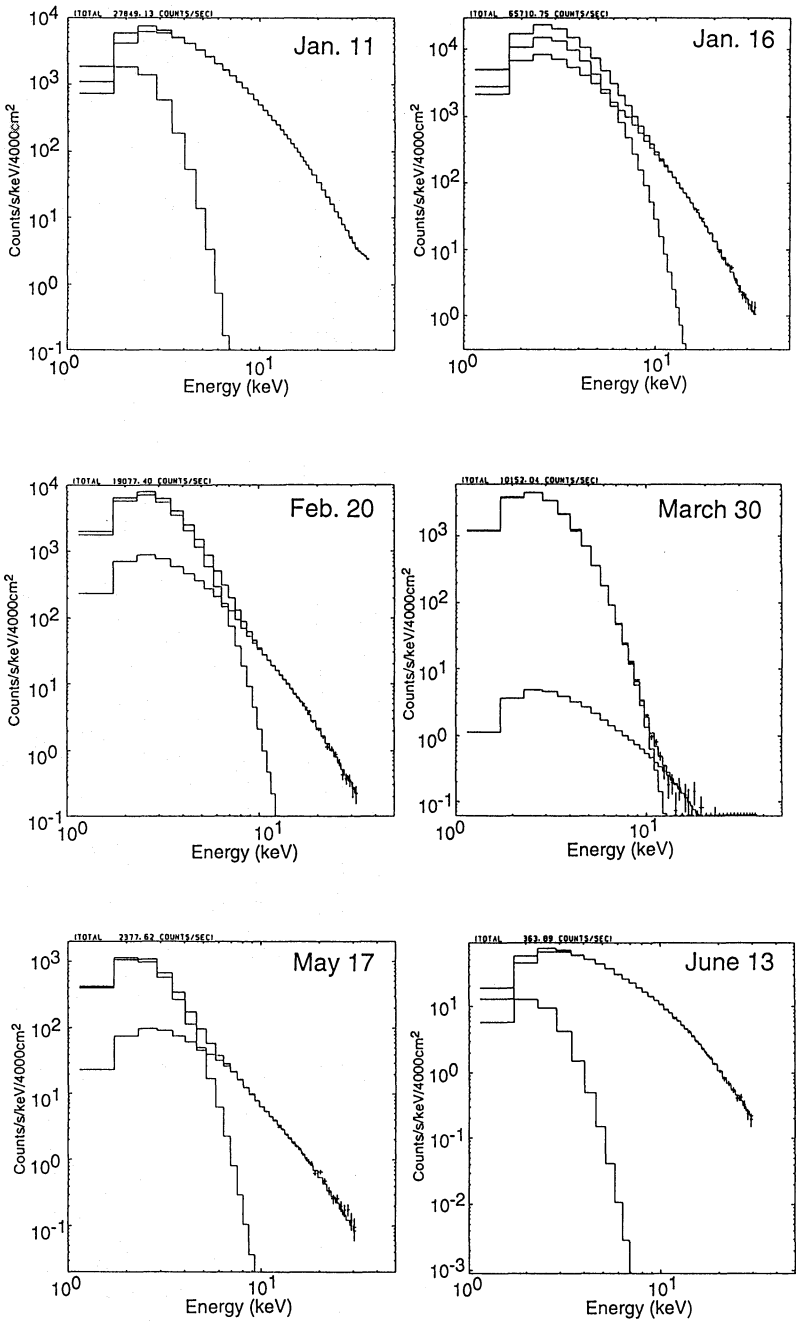

Fig. 14. Results of spectral fitting for energy spectra in the soft state (January 11, January 16, February 20, March 30, and May 17) and the hard state (June 13). The adopted model is the multicolor disk model (for the soft component) plus a power-law function × the smeared edge model (for the hard component). See the text for explanations of the model.

$M(t)]/\tau$, where $M(t)$ is the mass accreted from the outburst to a time t and $M(\infty)$ is the total mass accreted from the outburst to the diminution (although we assume τ is constant, this assumption should be carefully investigated; see Ichikawa, Osaki 1992). This simple relationship is suggestive of a "mass reservoir," such that the mass-loss rate from the reservoir $\dot{M}(t)$ is proportional to the mass stored at that time, $M(\infty)-M(t)$, and that the inverse of the proportional coefficient is the decay time τ.

The most probable candidate for the mass reservoir is an optically thick accretion disk around the central

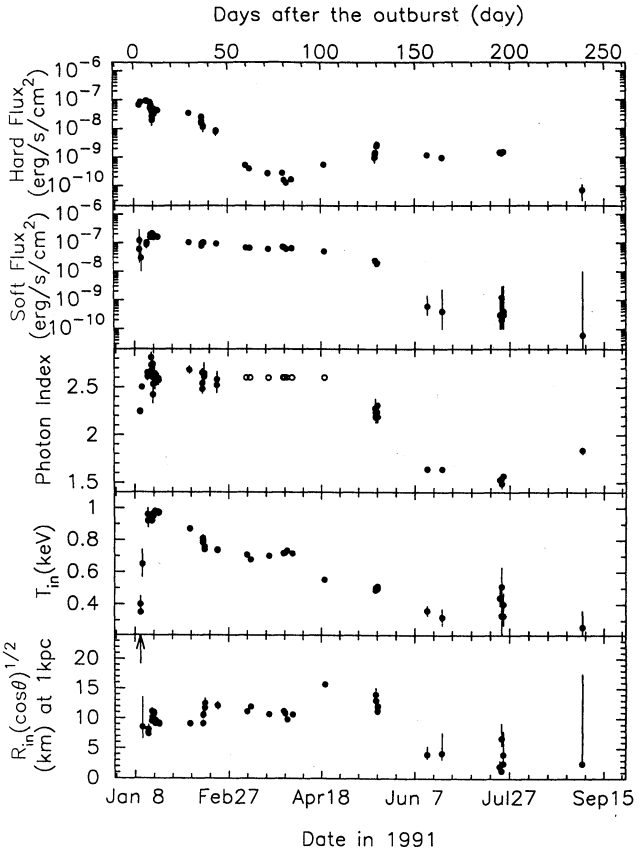

Fig. 15. Time variation of the best-fit values for the major parameters of the spectral fitting. The photon-index of the power-law component is fixed for the data obtained in March and April (shown with open circles). The energy flux of the power-law component is calculated for 2–20 keV, and the multicolor disk flux is the bolometric one calculated using the formula $2\,\sigma(r_{\rm in}\sqrt{\cos\theta}\,/d\,)^2\,T_{\rm in}{}^4$.

object. The mass stored in the accretion disk may fall within a relatively short time ($\sim$ 300 d) due to, for example, a thermal instability of the accretion disk (Cannizzo et al. 1985; Huang, Wheeler 1989; Mineshige, Wheeler 1989; Mineshige et al. 1993). As the total mass and surface density of the disk increase, the viscosity becomes larger, as does the mass accretion rate, if the size of the accretion disk is kept nearly constant. The proportion of the mass accretion rate to the stored mass in the reservoir can thus be qualitatively understood. Mineshige, Yamasaki, and Ishizaka (1993) showed, with a precise disk structure calculation, that the exponential disk luminosity decay can be explained if the mass and angular momentum are removed from the disk at a constant rate, and a thermal instability is actually supposed to induce such a constant mass and angular momentum removal. Since the exponential light curve and the $\sim$ 30 d decay time are common characteristics in the decay phase of the black-hole candidate X-ray novae A0620−00, GS 2000+25, and GS 2023+338 (figure 1, subsection 3.1), a common mechanism is presumed to be working for these sources.

The total-mass accreted during this outburst can be estimated based on the current observation with an assumed distance to the source. The distance was estimated to be $\sim$ 1.4 kpc by Della Valle, Jarvis, and West (1991a, b) and $\sim$ 8 kpc by Cheng et al. (1992), thus showing a large discrepancy. We tentatively adopt 2.5 kpc, which makes the inner accretion disk radius obtained from spectral fitting comparable to those of other black-hole candidates (see subsection 4.3). At the maximum, the luminosity is $\sim 1.9\times10^{38}(d/2.5\ {\rm kpc})^2\ {\rm erg\ s^{-1}}$, where we added the bolometric multicolor disk luminosity, assuming $\cos\theta = 1/2$, and the power-law luminosity within 2–100 keV, assuming isotropic emission. Accordingly, the mass-accretion rate at the peak is $\dot{M} \sim 2.5\times10^{18}(d/2.5\ {\rm kpc})^2\ {\rm g\ s^{-1}}$, assuming the efficiency to be 1/12 [$L_{\rm disk} = (1/2)GM\dot{M}/r_{\rm in} = (1/12)\dot{M}c^2$ where $r_{\rm in}$ is $3r_{\rm g}$.] Approximating the light curve up to and after the maximum as $\propto \exp(t/3\ {\rm d})$ and $\propto \exp(-t/30\ {\rm d})$, respectively, the total accreted mass is estimated as $\sim 7\times10^{24}(d/2.5\ {\rm kpc})^2$ g. On the other hand, integrating the surface density of an optically thick accretion disk in which free-free opacity dominates [(2.19) in Shakura and Sunyaev 1973] from $R_{\rm in}$ to $R_{\rm out}(\gg R_{\rm in})$, we can estimate the mass of the accretion disk as

$$M_{\rm disk} \approx 7\times10^{24}\left(\frac{0.2}{\alpha}\right)^{4/5}\left(\frac{\dot{M}_{\rm steady}}{5\times10^{15}\ {\rm g\ s^{-1}}}\right)^{7/10} \times\left(\frac{M}{6\,M_\odot}\right)^{1/4}\left(\frac{R_{\rm out}}{3\times10^{11}{\rm cm}}\right)^{5/4}. \quad (4)$$

Thus, the total mass required in the present outburst can be stored in an optically thick accretion disk around the black-hole with such reasonable parameters shown above (note that $\dot{M}_{\rm steady}$ in this formula is the steady mass transfer rate from the companion to the accretion disk and not immediately related to the X-ray emission in the inner part).

The recurrent time between outbursts may be determined by the total accreted mass ($\approx$ necessary mass to trigger the outburst) divided by the steady mass accretion rate, as $\sim 7\times10^{24}[{\rm g}]/5\times10^{15}[{\rm g\ s^{-1}}] \approx 40$ y. Although previous outbursts of GS 1124−68 have never been observed (with highly non-uniform photographic coverage), this time gives the correct order of the magnitude for the recurrence times of A0620−00 (58 y) and GS 2023+338 (51 y; but possibly shorter, see Richter 1989).

It should be noted that the optical maximum was January 11–12 (Della Velle et al. 1991a, b), $\sim$ 4 d earlier than the X-ray peak. The time difference may correspond to the time for the accreting matter to drift through the ac-

cretion disk from the optical light emission region to the X-ray emission region, if the disk instability transmits inward (note that there is also a model proposing that the disk instability transmits outward; see Chen et al. 1993). A similar optical peak advance to the X-ray peak ($\sim$ 20 d) was observed in periodic variations of LMC X-3 (Cowley et al. 1991).

The two humps $\sim$ 80 d and $\sim$ 200 d after the outburst were probably due to temporary increases in the mass-accretion rate. The temperature increase and invariance of the disk radius in the first hump support this idea.

4.2. Transition from the Soft State to the Hard State

The transition of GS 1124−68 from the soft (high) to the hard (low) state is the first clear spectral transition observed from X-ray novae. This transition is considered to have occurred between May 18 (the source was still in the soft state) and June 13 (the source was already in the hard state). As has been proposed for Cyg X-1 and GX 339−4, it is likely that the high-low transition was triggered by a change in the mass-accretion rate through a change in the surface density of the disk (e.g., Ichimaru 1977; Inoue, Hoshi 1987; Hoshi, Inoue 1988). In this scheme, when the accretion rate is larger than the critical accretion rate $\dot{M}_{\rm C}$, the inner part of the accretion disk is geometrically thin and optically thick [soft (high) state]; on the other hand, the disk turns geometrically thick and optically thin when $\dot{M} < \dot{M}_{\rm C}$ [hard (low) state].

The mass-accretion rates in GS 1124−68 before and after the transition are $\sim 3.4\times10^{17}(d/2.5\ {\rm kpc})^2$ g s^{-1} (May 17–18) and $\sim 3.1\times10^{16}(d/2.5\ {\rm kpc})^2$ g s^{-1} (June 13), respectively (as before, we added up the bolometric disk luminosity and the hard luminosity over 2 to 100 keV), so the transition seems to have occurred at around $\dot{M} \sim$ (5–10) $\times\ 10^{16}(d/2.5\ {\rm kpc})^2$ g s^{-1}. This is consistent with the critical mass accretion rate calculated by Inoue and Hoshi (1987), $\dot{M}_{\rm C} = 4.5\times10^{16}\alpha^{5/4}(M/M_\odot)$ g s^{-1}, with $M \sim 6M_\odot$ and $\alpha = 0.2$–0.5.

In the soft state, the optically thick accretion disk presumably extends to radii near to the black-hole. Since matter accretes in a quasi-stationary manner throughout the disk, short timescale variations of the disk component become relatively small (Miyamoto et al. 1993). The optical thickness may have a role to "stabilize" the accretion flow (Tanaka 1989). On the other hand, in the hard state the optically thick accretion disk presumably terminates far from the black-hole because of a thermal/viscous disk instability. Inside the optically thick disk, accreting matter may be fragmented into many rings, which would be a composite of the optically thick/geometrically thin part and the optically thin/geometrically thick part. This model nicely explains the X-ray shots in the hard-state of black-hole candidates (Miyamoto, Kitamoto 1989).

The hard component in the soft state and the energy spectrum in the hard state share apparent similarities, i.e., the power-law spectral shape (subsection 3.5) and large short-time variations (subsection 3.4). However, the differences in the power-law index (subsection 3.5), the differences in the power-density spectrum, and the phase-lag between different energy bands (Miyamoto et al. 1991a, b, 1993) all suggest that the physical mechanism of the power-law component is not completely identical in the two states.

4.3. Origin of the Soft Component

Subsection 3.5 describes how the energy spectra of GS 1124−68 throughout the observations were fitted with a two-component model, in which the soft component is the multicolor disk model and the hard component is a power-law function. However, the characteristic of the soft component is rather different for several periods.

From the outburst to the peak, the spectra showed an anti-correlation between the soft and hard energies, pivoting at $\sim$ 8 keV. This may be actually due to an anti-correlation between the two independent hard and soft spectral components; however, it can be alternatively explained by Comptonization, such that soft photons are produced by down-scattering of hard photons, or hard photons are made by up-scattering of soft photons. In the Comptonization scheme, the fact that the flux of the soft and hard components was comparable suggests that the Comptonization was saturated ($y \approx 1$). The softening of the energy spectrum is presumably due to a cooling of the Comptonizing plasma.

From the peak to the end of the soft state, according to the luminosity decay, the temperature of the multicolor disk component decreased from $T_{\rm in} \sim 0.98$ keV to ~ 0.50 keV; these values are distinguishably smaller than the typical values for neutron-star binaries ($\sim$ 1.4 keV; Mitsuda et al. 1984) but similar to those for other black-hole candidates (e.g., Makishima et al. 1986; Ebisawa et al. 1989; Treves et al. 1990; Ebisawa 1991; Ebisawa et al. 1993), exhibiting an "ultra-softness" of the energy spectra. In contrast, the size parameter of the disk was concentrated at about $r_{\rm in}\sqrt{\cos\theta} \sim 28\ (d/2.5\ {\rm kpc})$ km. This remarkable characteristic, namely, the invariance of the innermost radius of an optically thick accretion disk in spite of the large mass-accretion rate variation, is common to black-hole candidates LMC X-3 (Ebisawa et al. 1993) and GS 2000+25 (Tanaka 1989; Takizawa 1991; Ebisawa 1991). This suggests that the innermost disk radius is directly related to the mass of the central object (Ebisawa et al. 1991; Ebisawa 1991; Tanaka 1991). It has been pointed out that, compared with the energy spectra of black-hole candidates and low mass X-ray binaries, the size parameter of the multicolor disk model $r_{\rm in}\sqrt{\cos\theta}$ is generally larger for black-hole candidates (typically 20–35 km) than for low-mass X-ray bina-

ries (typically 5–15 km), presumably reflecting difference in the masses of the central objects (Makishima 1984; Inoue 1985; Makishima et al. 1986; Ebisawa 1991; Tanaka 1991; Yaqoob et al. 1993). A comparison of the $r_{\rm in}\sqrt{\cos\theta}$ value of GS 1124−68 [$\sim$ 28 km (d/2.5 kpc)] with typical values for other black-hole candidates suggests the distance is actually more likely to be 2–3 kpc than 1.4 kpc (Della Valle et al. 1991a, b) or 8 kpc (Cheng et al. 1992).

In the multicolor disk model, although the local emission of the disk is assumed to be the blackbody, this would not be precisely correct. In the inner region of the disk, a hot outer layer would significantly affect the emergent spectra by Comptonization (Shakura, Sunyaev 1973). As has been studied concerning X-ray burst energy spectra, such a Comptonized spectrum would form the Wien peak, and the spectrum within 2–20 keV may be approximated with the diluted Planckian, $I(E) = (T_{\rm eff}/T_{\rm col})^4 B(T_{\rm col}, E)$, where $T_{\rm col}$ and $T_{\rm eff}$ are the color and effective temperature, respectively. In the diluted Planck spectrum, the spectral shape is the same as the Planckian with $T_{\rm col}$, which is larger than $T_{\rm eff}$; however, the normalization is smaller by the factor of $(T_{\rm col}/T_{\rm eff})^4$. The $T_{\rm col}/T_{\rm eff}$ value is $\sim$ 1.5 in the case of X-ray bursts (e.g., Ebisuzaki et al. 1984; London et al. 1986). If this approximation holds, and the color to the effective temperature ratio $T_{\rm col}/T_{\rm eff}$ is constant along the disk radius, the multicolor disk model should still be valid. In that case, the temperature $T_{\rm in}$ of the multicolor disk model is the color temperature and the effective temperature is smaller by the factor $T_{\rm col}/T_{\rm eff}$; also, the actual disk size should be $(T_{\rm col}/T_{\rm eff})^2$ times larger than the $r_{\rm in}$ obtained using the multicolor disk model.

The fact that $r_{\rm in}\sqrt{\cos\theta}$ does not systematically change during the luminosity decay indicates that $T_{\rm col}/T_{\rm eff}$ is fairly stable against any luminosity variation. However, the failure of the multicolor disk model regarding the March-April spectra may suggest that $T_{\rm col}/T_{\rm eff}$ is not constant along the disk radius, but is variable. More precise accretion-disk models are needed to model the observed data by solving the radiative transfer taking account of Comptonization.

The $r_{\rm in}$ value obtained from the model fitting may be related to the mass of the central object. The actual disk size should be $\sim r_{\rm in}(T_{\rm col}/T_{\rm eff})^2$, as stated above; this could correspond to the radius at which the effective temperature becomes maximum, that is $(7/6)^2$ times the actual inner disk radius 3 $r_{\rm g}$. (Shakura, Sunyaev 1973). From this relationship we obtain

$$M \approx 1.9 \left(\frac{r_{\rm in}\sqrt{\cos\theta}}{10\ {\rm km}}\right)\left(\frac{T_{\rm col}/T_{\rm eff}}{1.5}\right)^2\left(\frac{1/2}{\cos\theta}\right)^{1/2} M_\odot,$$
$$\approx 7.4 \left(\frac{T_{\rm col}/T_{\rm eff}}{1.5}\right)^2\left(\frac{d}{2.5\ {\rm kpc}}\right)\left(\frac{1/2}{\cos\theta}\right)^{1/2} M_\odot, \quad (5)$$

where we use $r_{\rm in}\sqrt{\cos\theta}$ = 27.5 km (d/2.5 kpc). A comparison of the multicolor disk model with a more precise model which takes account of both special and general relativity (Hanawa 1989) shows that the thus-estimated mass becomes smaller due to relativistic effects. Using the relation between the mass of the central object and the multicolor disk parameter, while taking into account the relativistic effects (Ebisawa 1991; Ebisawa et al. 1991), we obtain

$$M \approx 6.0 \left(\frac{T_{\rm col}/T_{\rm eff}}{1.5}\right)^2\left(\frac{d}{2.5\ {\rm kpc}}\right) f(\theta)\ M_\odot, \quad (6)$$

where $f(60°) = 1$ and $f(0°) = 0.46$ (minimum).

After a transition to the hard state, the energy spectra could be represented by a power-law function over almost the entire energy range; further the multicolor disk component appeared as a minor "soft excess" below $\sim$ 3 keV. Such soft excess components have been also found in the hard state of Cyg X-1 (Kitamoto et al. 1984; Barr, van der Woerd 1989; Balucinska, Hasinger 1991), GX 339−4 (Ilovaisky et al. 1986; Ueda et al. 1994), and GS 2023+338 (Yoshida 1990; Tanaka 1990). The soft excess component of GS 1124−68 was variable over a timescale of several tens of minutes (figure 11), and the variation was mainly associated with the size parameter rather than the temperature, contrary to the situation during the decay phase in the soft state. This suggests a different origin of the soft excess component from the optically thick accretion-disk component in the decay phase of the soft state. Optically thin emission far from the central engine is proposed as being the origin of the soft excess component, on the basis that it is free from absorption by intervening matter of the central source, and that the temperature is common to the soft excess component in Active Galactic Nuclei (Inoue 1992). However, the fast variation observed for GS 1124−68 might rule out an optically thin origin.

4.4. *Origin of the Hard Component*

The following observational facts are probably important when investigating the origin of the hard component: (1) The hard component is represented by a power-law function, and the photon index is 2.2–2.6 in the soft state and 1.5–1.7 in the hard state; (2) in the soft state, the hard component varies largely (about three orders of magnitude) and independently of the soft component with long timescales (days–months); (3) the hard component shows significant short-time variations down to $\sim$ ms in both the soft and hard states; (4) on one occasion while in the soft state, an emission line at around 500 keV, probably due to electron-positron annihilation, was observed by the GRANAT satellite (Gil'fanov et al. 1991; Sunyaev et al. 1992; Goldwurm et al. 1992; Gil'fanov et al. 1993; Goldwurm et al. 1993; Lund 1993). These char-

acters of the hard component [except (4)] are common to other black-hole candidates (Miyamoto et al. 1991a, b; Ebisawa 1991).

Often, low mass neutron-star binaries in their low-intensity state show hard power-law like energy spectra within about the 2–20 keV energy range (e.g., White et al. 1988; Mitsuda et al. 1989; Yoshida 1993). However, the annihilation lines, as well as the high energy X-rays above ~ 100 keV, have never been reported from low mass neutron-star binaries. Electron-positron annihilation becomes significant when there are many hard photons with energy above 2×511 keV, and the compact parameter $l \equiv L\sigma_{\rm T}/Rm_{\rm e}c^3 > 20\pi$ (e.g., Lightman, Zdziarski 1987). The luminosity when the electron-positron annihilation line was detected (January 20) was $\sim 3 \times 10^{37}(d/2.5\ {\rm kpc})^2$ erg s^{-1}, integrating the power-law function of the index 2.6 from 2 to 500 keV. We thus obtain $R < 140\ {\rm km}\ (d/2.5\ {\rm kpc})^2$ from the condition $l > 20\pi$. This small size suggests that there is a mechanism just in the vicinity of the black-hole to yield power-law photons by releasing gravitational energy.

It seems very difficult to explain that the hard component in the soft state varied independently of the soft component on timescales of days to months. If there is a mechanism near to the inner edge of an optically thick accretion disk that modulates the mass-flow inwards and accordingly the hard component intensity, the independent variation of the hard component may be explained. In this case, the long timescales of the hard component must be created by an unknown mechanism in the vicinity of the black-hole where the dynamical timescales are much shorter. Alternatively, the long timescales may originate in a modulation of the mass flow at outer parts of the accretion disk or the companion star, where the dynamical timescale will be sufficiently long. However, in this case, it is enigmatic that the soft component is not affected by that modulation and does not vary together with the hard component.

4.5. Broad Absorption Structure in the Energy Spectra

In both the soft and hard states, a broad absorption structure was observed over the 7–20 keV energy range of the hard component. In the present work, the broad absorption structure was fitted with the smeared edge model, in which the original iron K-edge structure was modified taking into account an artificial smearing effect; actually, however, disk reflection (e.g., Guilbert, Rees 1988; Lightman and White 1988) or a partial absorption mechanism (e.g., Matsuoka et al. 1990; Yoshida et al. 1993) may be yielding the broad absorption structure. In terms of the disk reflection model, the smeared edge energy $E_{\rm edge}$ and the depth of the edge $N_{\rm Fe}$ give a rough measure of the ionization state of the disk and the amount of reflection, respectively. Around the maximum intensity (January 16), $E_{\rm edge}$ was ~ 7.7 keV; on the other hand, it was consistent with 7.1 keV (K-edge energy of neutral iron) in the hard state. This variation of the edge energy suggests that the disk is more ionized when the X-ray luminosity is higher, probably due to the high temperature of the disk and X-ray irradiation. Furthermore, the $N_{\rm Fe}$ values in the soft state (~ 19.9 cm^{-2}; note that the absolute values of $N_{\rm Fe}$ have no meaning since the model is artificial) is significantly larger than those in the hard state (19.1–19.5 cm^{-2}). This suggests that the amount of reflection is larger for the soft state, and implies that the solid angle of the disk relative to the incident X-rays is larger in the soft state. This is consistent with the picture shown in subsection 4.2 that the optically thick accretion disk extends down to near the black-hole in the soft state, but terminates far outside in the hard state.

In the course of the reflection, an iron fluorescence K-line is necessarily emitted at around 6.4 keV, accompanying the iron K-ionization. However, because of the limited counter energy resolution and the coupling of the line and edge structure, we could not clearly detect the emission lines in the present analysis. Precise reflection models should be applied in order to investigate the emission lines as well as the ionization state of the reflector. This is an important subject left for future study.

5. Conclusion

We observed the bright X-ray nova GS 1124−68, a promising black-hole candidate having dynamical evidence of large mass of the central compact object (Remillard et al. 1992). The observations were made between 1991 January 10, two days after the discovery, and 1991 September 3. Although subsequent observations were carried out on September 24 and October 16, the source was not detected below the detection limit (~ 0.3 mCrab).

The important results are summarized as follows:

(1) GS 1124−68 reached its maximum luminosity eight days after the outburst; the luminosity then decayed exponentially with an e-folding time of ~ 30 d. Temporary luminosity increases were found ~ 80 d and ~ 200 d after the outburst. These characteristics are shared with black-hole candidate novae A0620−00, GS 2000+25, and GS 2023+338.

(2) GS 1124−68 exhibited a drastic state transition between May 18 and June 13 that was quite similar to the high-low transition thus far observed from Cyg X-1 and GX 339−4. Before the transition, the energy spectra were relatively soft and the short-term variations were small; after the transition, the energy spectra became much harder and intense short-term variations akin to those of Cyg X-1, GX 339−4, and GS 2023+338 became prominent.

(3) From the first observation on January 10 to the X-ray peak on January 16, a clear anti-correlation between soft and hard X-ray energies was observed with the spectral pivot at around 8 keV. This may have been due to Comptonization, such that soft photons are produced by down-scattering of hard photons, or hard photons are made by the up-scattering of soft photons.
(4) The energy spectra after the peak up to the end of the soft state comprise a soft thermal component which is considered to originate in the optically thick accretion disk and a hard power-law component which is dominant above ~ 7 keV. Although the soft component gradually decreased, the hard component showed significant variations over a wide range of timescales from sub-seconds to months, independently of the soft component.
(5) Until early February, during which period the ~ 6 Hz QPO and time lags between different energy bands were observed (Dotani 1992; Miyamoto et al. 1993), the intensity of the hard component was comparable to that of the soft component. After that, the hard component gradually decayed and could hardly be detected at the end of March to early April. Time variations shorter than several hundred seconds became less conspicuous as the hard component decreased. In May, the hard component became significantly larger again, accompanied by increases in the short-term variations.
(6) In our spectral model for the decay phase in the soft state, although the disk temperature decreased from 0.98 to 0.5 keV, the innermost radius of the disk stayed within a narrow range without showing systematic variations. By comparing the innermost disk radius with those of other black-hole candidates, the distance to the source is inferred to be 2–3 kpc. The outburst and state-transition mechanism is consistently explained in terms of the optically thick accretion-disk model with $M \approx 6M_{\odot}$ at $d \approx 2.5$ kpc.
(7) After the transition to the hard state, the energy spectra became much harder and roughly expressed with a single power-law function. A small soft-excess component was additionally observed below ~ 3 keV.
(8) The spectral index of the hard component was 2.2–2.7 in the soft state, and decreased to ~ 1.7 in the hard state, showing an intriguing contrast. This change may be a consequence of a difference in the hard X-ray production mechanism between the two states.
(9) A broad absorption structure was observed both in the soft and hard states above ~ 7 keV whenever there was a significant amount of hard X-rays. This structure may be explained based on the reflection of X-rays by an optically thick accretion disk. From the edge energy and depth, it is inferred that the disk is more ionized and has a larger solid angle in the soft state than in the hard state.

Being a confident black-hole candidate with evidence of large mass of the compact object (Remillard et al. 1992), GS 1124−68 has shown almost all the X-ray characteristics which have been considered to be inherent to black-hole candidates. GS 1124−68 confirms that these X-ray properties are consequences of the central object being a black-hole, not a neutron-star, and provides observational ground upon which we may judge an X-ray binary to be a black-hole system only from X-ray observations.

The authors acknowledge Prof. N. Shibazaki for variable discussions. We also thank all the members of the Ginga team for making the GS 1124−68 observations available as a target of opportunity.

References

Balucinska M., Hasinger G. 1991, A&A 241, 439
Bar P., van der Woerd H. 1989, ApJL 352, L41
Brandt S. et al. 1992, A&A 254, L39
Cannizzo J.K., Wheeler J.C., Ghosh P. 1985, in Proc. Cambridge Workshop on Cataclysmic Variables and Low-Mass X-ray Binaries, ed D.Q. Lamb, J. Patterson (Reidel, Dordrecht) p307.
Casares J., Charles P.A., Naylor T. 1992, Nature 355, 614
Chen W. et al. 1993, ApJ 408, L5
Cheng F.H. et al. 1992, ApJ 397, 664
Cowley A.P. et al. 1991, ApJ 381, 526
Della Valle M., Jarvis B.J., West R.M. 1991a, A&A 247, L33
Della Valle M., Jarvis B.J., West R.M. 1991b, Nature 353, 50
Done C., Mulchaey J.S., Mushotzky R.F., Arnaud K.A. 1992, ApJ 395, 275
Dotani T. 1989, Doctoral Thesis, University of Tokyo (ISAS Research Note 418) (ISAS, Sagamihara)
Dotani T. 1992, in Frontiers of X-ray Astronomy, ed by Y. Tanaka, K. Koyama (Universal Academy Press, Tokyo) p151
Ebisawa K. 1991, Doctoral Thesis, Tokyo University (ISAS Research Note 483) (ISAS, Sagamihara)
Ebisawa K., Mitsuda K., Hanawa T. 1991, ApJ 367, 213
Ebisawa K., Mitsuda K., Inoue H. 1989, PASJ 41, 519
Ebisawa K. et al. 1993, ApJ 403, 684
Ebisuzaki T., Hanawa T.,Sugimoto D. 1984, PASJ 36, 551
Elvis M., Page C.G., Pounds K.A., Ricketts M.J., Turner M.J.L. 1975, Nature 257, 656
Gil'fanov M. et al. 1991, Soviet. Astron. Lett. 17, 437
Gil'fanov M. et al. 1993, A&AS 97, 303
Goldwurm A. et al. 1992, ApJL 389, L79
Goldwurm A. et al. 1993, A&AS 97, 293
Guilbert P.W., Rees M.J. 1988, MNRAS 233, 475
Hanawa T. 1989, ApJ 341, 948
Hoshi R., Inoue H. 1988, PASJ 40, 421
Huang M., Wheeler J.C. 1989, ApJ 343, 229
Ichikawa S., Osaki Y. 1992, PASJ 44, 15
Ichimaru S. 1977, ApJ 214, 840
Ilovaisky S.A. et al. 1986, A&A 164, 67
Inoue H. 1985, Space Sci. Rev. 40, 317
Inoue H. 1989, in Proc. 23rd ESLAB Symp. on two topics in X-ray astronomy, vol.2 (ESA, Paris) p7

Inoue H. 1992, in Frontiers of X-ray Astronomy, (Universal Academy Press, Tokyo) p291
Inoue H., Hoshi R. 1987, ApJ 322, 320
Kaluzienski L.J. et al. 1977, ApJ 212, 203
Kitamoto S. et al. 1984, PASJ 36, 731
Kitamoto S. et al. 1990, Nature 342, 518
Kitamoto S., Tsunemi H., Miyamoto S., Hayashida K. 1992, ApJ 394, 609
Lightman A.P., White Y.R. 1988, ApJ 335, 57
Lightman A.P., Zdziarski A.A. 1987, ApJ 319, 643
London R.A., Taam R.E., Howard W.M. 1986, ApJ 306, 170
Lund N. 1993, A&AS 97, 289
Lund N., Brandt S. 1991, IAU Circ. 5161
Makino F., the Ginga team 1991, IAU Circ. 5161
Makishima K. 1984, in X-ray Astronomy '84, ed M. Oda, R. Giacconi (Institute of Space and Astronautical Science, Tokyo) p165
Makishima K. et al. 1986, ApJ 308, 635
Matsuoka M., Piro L., Yamauchi M., Murakami T. 1990, ApJ 361, 440
McClintock C.K., Remillard R.A. 1986, ApJ 308, 110
McMaster W.H. et al. 1970, Compilation of X-ray Cross Sections, UCRL-50174
Mineshige S., Wheeler J.C. 1989, ApJ 343, 241
Mineshige S., Yamasaki T., Ishizaka C. 1993, PASJ 45, 707
Mitsuda K. et al. 1984, PASJ 36, 741
Mitsuda K. et al. 1989, PASJ 41, 97
Miyamoto S., Kimura K., Kitamoto S., Dotani T., Ebisawa K. 1991a, ApJ 383, 784
Miyamoto S., Kitamoto S. 1989, Nature 342, 773
Miyamoto S., Kitamoto S., Iga S., Negoro H., Terada K. 1991b, ApJL 391, L21
Miyamoto S., Iga S., Kitamoto S., Kamado Y. 1993, ApJL 403, L39
Morrison R., McCammon D. 1983, ApJ 270, 119
Nishimura J., Mitsuda K., Itoh M. 1986, PASJ 38, 819
Piro L., Yamauchi M., Matsuoka M. 1990, ApJL 360, L35
Pounds K. et al. 1990, Nature 344, 132
Remillard R.A., McClintock J.E., Bailyn C.D. 1992, ApJL 399, L145
Richter G. A. 1989, Inf. Bull. Variable Stars, No.3362
Shakura N.I., Sunyaev R.A. 1973, A&A 24, 337
Sunyaev R.A. et al. 1992, ApJL 389, L75
Takizawa M. 1991, Master Thesis, Tokyo University (in Japanese)
Tanaka Y. 1989, in Proc. 23rd ESLAB Symp. on two topics in X-ray astronomy, vol.1 (ESA, Paris) p3
Tanaka Y. 1990, in Iron Line Diagnostics in X-ray sources, ed A. Treves (Springer-Verlag, Berlin)
Tanaka Y. 1991, in The Symposium on X-ray Binaries and the Formation of Binaries and Millisecond Radio Pulsars, (University of California, Santa Barbara)
Treves A. et al. 1990, ApJ 364, 266
Tsunemi H. et al. 1989, ApJL 337, L81
Turner M.J.L. et al. 1989, PASJ 41, 345
Ueda Y., Ebisawa K., Done C. 1994, PASJ 46, 107
White N.E., Kalzienski J.L., Swank J.H. 1984 in High Energy Transients in Astrophysics, ed S.E. Woodley (AIP Conference Proceedings No.115), (AIP, New York) p31
White N.E., Marshall F.E. 1984, ApJ 281, 354
White N.E., Stella L., Parmar A.N. 1988, ApJ 324, 363
Yaqoob T., Ebisawa K., Mitsuda K. 1993, MNRAS 264, 411
Yoshida K. 1990, Master Thesis, Tokyo University (in Japanese)
Yoshida K. et al. 1993, PASJ 45, 605